International Journal of Nanoscience
Vol. 2, Nos. 4 & 5, (2003) 375-379

World Scientific
Connecting Great Minds

FABRICATION AND MODELING OF MICROCHANNEL MILLING USING FOCUSED ION BEAM

A. A. TSENG, B. LEELADHARAN, B. LI, I. A. INSUA
Department of Mechanical and Aerospace Engineering, Arizona State University
Tempe, Arizona 85287-6106, USA

C. D. CHEN
Institute of Physics, Academia Sinica,
Nankang, Taipei, Taiwan 11529 ROC

The capability of using the Focused Ion Beam (FIB) for milling micro-channels is experimentally and theoretically investigated. Microchannel structures are fabricated by a NanoFab 150 FIB machine, using an arsenic (As^{2+}) ion source. A beam current of 5-pA at 90-keV accelerating energy is used. Several microchannel patternings are milled at various dwell times at pixel spacing of 14.5 nm on top of a 60-nm gold-coated silicon wafer. An analytical/numerical model is developed to predict the FIB milling behavior. By comparing with the experimental measurements, the model predictions have been demonstrated to be reliable for guiding and controlling the milling processes.

Keywords: Focused ion beam, Gold film, Microchannel, Micromachining, Modeling, Milling, Nanofabrication, Redeposition, Sputtering.

1. Introduction

The Focused Ion Beam (FIB) has been a valuable tool in semiconductor industry for repairing masks and individual metal lines in integrated circuit production, and for doping semiconductors. Microstructures of various geometries, including scanning microprobes, micro-beams, micro-lens, and micro-gears, have been successfully fabricated using FIB. The objective of the paper is to study the FIB milling profile. The milling experiments are first conducted by changing the dwell time to obtain different sizes of microchannels. Milled profiles are measured using an Atomic Force Microscope (AFM). A two-dimensional model is then developed taking into account several effects, including sputtering, redeposition, and dynamic profile changes. Finally, the theoretical model is verified by comparing the model prediction with experimental observations.

2. Experiment

The FIB machine: Nano-FAB Model 150 from Nanofab of Columbia, Maryland, is used for the present experimental study. The interchangeable liquid-metal ion

sources provide several different ion species, including PdAsB, AuSiBe, and Ga. The beam voltage can be adjusted from 4 to 150 kV with current densities up to 5 A/cm^2. The beam diameters can be controlled in the range from 50 to 500 nm.

In the experiment, the target substrate is a silicon wafer, coated with a gold film of 60-nm thick. To mill a micro-channel, the ions are focused onto a series of adjacent spots. The pixel spacing must be small enough to allow a proper overlap between adjacent pixels so that a continuous channel can be milled. A 90-keV As^{2+} FIB with a beam current of 5 pA is selected in the present study. The PdAsB alloy is used as the source to provide the As^{2+} ion beam. The double-charged As ions accelerated in a 45-kV differential potential are used to achieve the 90-keV beam energy. The pixel spacing (p_s) is set at 14.5 nm and the beam FWHM diameter (d_f) is at 50 nm. The dwell time is varied from 5 to 50 ms.

An AFM image of a milled channel pattern "ASU" is shown in Fig 1. The corresponding channel cross-section profiles at several different locations are shown in Fig. 2. The channel profiles are somewhat symmetric and only the right half of the profiles are presented. A correlation curve for all the measurements is also shown in the figure. The curve is based on a 6th order polynomial with the correlation coefficient (R) being 0.994, which means the two variables, the channel depth and radial location, correlate extremely good. The deviations shown in the figure, although less than 10 % of their central depth, can come from many sources. Since the measurements are taken from different sections and each section may have different crystal orientation, the anisotropic effects of the substrate materials can cause the deviations. Furthermore, the instability of the beam current and beam movement during milling may also be the sources for the variations of the channel profile.

To establish the reliability of the measurements, the profiles of the milled channels are examined by two types of scanning resolutions (E and J scans) and two types of tips (17° and 35°) when using the AFM. The digital image from the E-scan has nearly 12 times higher the resolution than that of the J-scan. The 35°-tip is normally used for general-purpose planar scanning while the 17° one is for

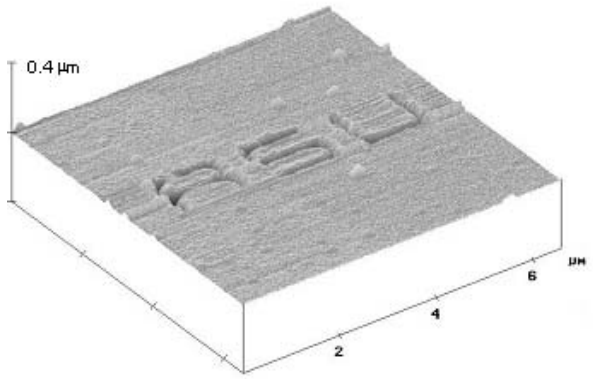

Fig. 1. AFM image of FIB milled pattern using E-scan with 17°-tip

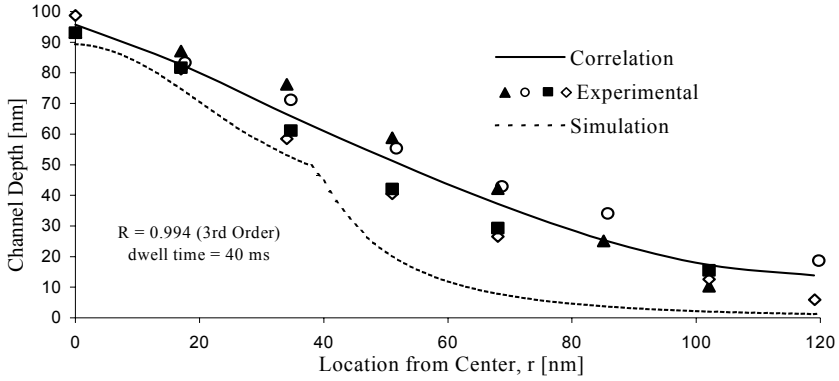

Fig. 2. Milled channel profile using E scan with 17° tip

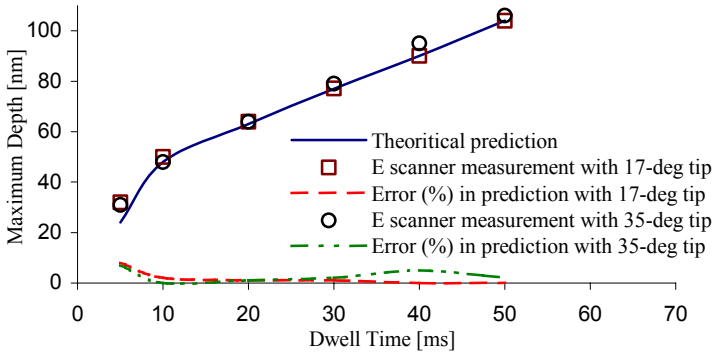

Fig. 3. Comparison of maximum channel-depth prediction with E-scanner measurement.

higher aspect-ratio structures. Since the effect of using these two different tips with two different scanning resolutions on the measurement are insignificant as shown in Fig. 3, the data presented in Fig. 2 should be considered reliable and consistent. The main reason for this insignificant effect on the measurement should be due to the fact that the milled channels are relatively shallow and both tips can deliver consistent results. Also, the channels sizes are not too small so that the resolution of a J-scan is good enough to provide reliable results. Figures 1 and 2 show the results based on an E scan with a 17°-tip.

3. Modeling

A FIB milling model considering the ion sputtering and redeposition of the sputtered atoms is developed to predict the profile of the milled channel for a substrate made of one or two materials. The main input parameters to the model are the properties of the substrate, the kind of ion species used, the FIB beam parameter settings, and the milling operating parameters.

In modeling, the ion density distribution rate of a FIB (Y) is mathematically represented by a Gaussian distribution:[1,2]

$$Y(r,\sigma) = \frac{Q_t}{2\pi\sigma^2}\exp\left(-\left(\frac{r}{\sigma\sqrt{2}}\right)^2\right) \qquad 0 \leq r < \infty \qquad (1)$$

where Y is the number of the ions per unit area per unit milling time; Q_t is the total number of ion dose per unit milling time; r is the radial coordinate and the beam center is located at r = 0; and σ is the standard deviation of the Gaussian distribution, in which the beam FWHM diameter (d_f) is equal to 2.355σ. By satisfying the law of the conservation of energy, Q_t can be found to be $I_p/(nC_e)$, where I_p is the beam current, C_e is the charge of one electron or single-charged ion equal to $1.60\text{x}10^{-19}$ C, and n is the number of charge, in which n = 1 is for single charged ion beams while n = 2 is for double charged ion beams.

Theoretically, as indicated in Eq. (1), the Gaussian beam impinges an infinite target area. In modeling, only the region within the 6σ (six standard deviation) is considered, since the area within 6σ covers more than 99% of the ions impinging on the substrate. Then the area modeled is discretized into many unit cells or elements, similar to the scheme used in the finite difference or finite element methods. The amount of ions falls on this unit cell is assumed uniform and can be calculated. The amount of charges is used as the input for the calculation of the amount of sputtering. The sputtered volume (ΔS_{ij}) from the unit cell (i,j) can be estimated[2]:

$$\Delta S_{ij} = \eta(E_e,\theta)\delta v_s \delta t_d \Delta Q_{ij} \qquad (2)$$

where $\eta(E_e,\theta)$ is the sputtering yield; δv_s is the volume of one target atom occupied in the substrate; δt_d is the milling time step selected in the simulation; ΔQ_{ij} is the total number of ions per unit milling time that goes into the unit cell (i,j) and can be obtained by integrating the ion density distribution rate, given in Eq. (1), with respect to the unit cell area (ΔA_{ij}). Here, $\eta(E_e,\theta)$, the sputtering yield, is a function of the incident angle (θ) and ion energy (E_e) as well as the type of the ion source and target material. The function $\eta(E_e,\theta)$ can be obtained from a software, called SRIM[3]. For example, the sputtering rates at normal incidence for 90-keV arsenic ions on the gold and silicon targets can be calculated from SRIM as 17.8 and 3.1 atoms/ion, respectively. Also, the volume of a target atom (δv_s) can be estimated from information available in most material handbooks. For instance, since both the gold and silicon have a face-centered cubic (FCC) crystalline structure and each of their unit cells contains four atoms, one can find that $\delta v_s = b^3/4$, where b is the lattice parameter that is 0.40786 nm for Au and 0.54307 nm for Si. The number of the unit cells used in a simulation is typically from 1,000 to 10,000. The time step (δt_d) selected in a simulation is about one tenth of one duration time (t_d).

The second major part of the model is to consider redeposition. The model assumes that the amount of the sputtered atoms or ions from a source unit cell (i,j) to redeposit onto a target unit cell (k,l) is dependent on the relative locations

between the source and target cells as well as their own orientations. Two angles between the source and target cells are used to determine the amount of redeposition that will occur. The redeposited volume (ΔR_{ij}) can be found from the formula:[4]

$$\Delta R_{ij} = \frac{F(\beta) - F(\alpha)}{F(180^0)} \Delta S_{ii} \qquad \text{where: } F(x) = \frac{\pi r^3}{3}[\cos^3(x) - 3\cos(x) + 2] \tag{3}$$

Here, the angles α and β are, respectively, the minimum and maximum angles that are measured from the center of the source cell (i,j) to any possible locations within the target unit cell (k,l)[4]. Thus, the angle difference (β - α) defines the maximum projection angle of the target cell (k,l) onto the source cell (i,j). For a cell (k,l), the redeposition volume is calculated as the summation of contribution from all other source cells (i,j). The total displacement after redeposition is assumed to be normal to the surface of the unit cell.

4. Comparison

The model is verified by comparing its predictions by with the experimental measurement as shown in Fig 3 for different dwell times considered. The comparison shows that the model prediction agrees very well with the measurement; the maximum difference is less than 6 nm and decreases as the dwell time increases.

References

1. G. Ben Assayag, C. Vieu, J. Gierak, P. Sudraud, and A. Corbin, *J. Vac. Sci. Technol. B* **11**, 2420 (1993).
2. A. A. Tseng, I. A. Insua, J. S. Park, B. Li, and G. P. Vakanas, *J. Vac. Sci. Technol. B* **22**, 82 (2004).
3. J. P. Biersack and L. G. Haggmark, *Nuclear Instruments and Methods* **174**, 257 (1980).
4. F. Itoh, A. Shimase, and S. Haraichi, *J. Electrochem. Soc.* **137**, 983 (1990).